

pubs.acs.org/acscatalysis Research Article

Multi-Center Cooperativity Enables Facile C—C Coupling in Electrochemical CO₂ Reduction on a Ni₂P Catalyst

Shisheng Zheng,§ Xianhui Liang,§ Junjie Pan, Kang Hu, Shunning Li,* and Feng Pan*



Cite This: ACS Catal. 2023, 13, 2847-2856



Read Online

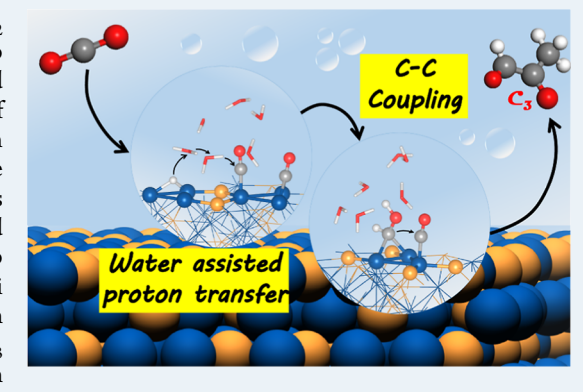
ACCESS I

Metrics & More

Article Recommendations

Supporting Information

ABSTRACT: The increasing interest for renewable electricity-driven CO₂ electroreduction calls for effective strategies in catalyst design, which have so far mainly focused on the compositional modulation such as doping and alloying. Recently, attention has turned to the microstructural tailoring of catalytic centers with a multi-center architecture to promote the formation of multi-carbon products, but theoretical understanding lags far behind the experimental discoveries. Herein, a systematic first principles study is performed on the representative electrocatalyst, Ni₂P, which is characterized by densely distributed Ni₃ catalytic centers and displays high selectivity to C-C coupling during CO₂ reduction reaction (CO₂RR). Not only the Ni atoms in each trinuclear Ni₃ site can cooperatively accommodate reaction intermediates for better opportunities of their coupling, but the adjacent Ni₃ sites can also work in synergy to drive the highly endothermic hydrogenation



steps in forming critical multi-carbon species. At the core of this capability lies the participation of the hydrogen-bonding network of water in transferring surface protons between neighboring Ni₃ sites, which builds a kinetically feasible path to circumvent the thermodynamic penalty in an electrochemical step. This work uncovers the mechanism by which cooperativity arises in multi-center microstructures, with implications generally for the design of CO2RR electrocatalysts to obtain valuable chemicals.

KEYWORDS: CO₂ reduction, C-C coupling, density functional theory, multi-center cooperativity, hydrogen bonds

INTRODUCTION

During the last two decades, tremendous strides have been made in the exploitation of renewable resources such as solar, wind, and hydropower, which contribute to the sharply falling price for renewable electricity. Nowadays, the application of renewable electricity for chemical and fuel production is a much-heralded approach not only to tackle the intermittent nature of these natural energy sources but also to alleviate our overwhelming reliance on fossil fuels.² One of the most impressive accomplishments has been the realization of electrochemical CO₂ reduction into multi-carbon (C_{2+}) products that can serve as the building blocks for long-chain hydrocarbon, oxygenates, and polymers.3-5 Given the currently growing anthropogenic CO2 emissions, the electrochemical CO2 reduction reaction (CO₂RR) offers a seductive promise of closing the global carbon loop, and hence the investigation into efficient CO₂RR catalysts has become ever more demanding in recent years.^{6,7} While extensive efforts have been put into this field, most catalysts for electrochemical CO2RR possess low selectivity toward C_{2+} products. Yet, the less desirable C_1 products, such as CO, formic acid, methanol, and methane, are much easier to obtained in the reaction, with a Faradaic efficiency (FE) of nearly 100% achieved over some particular catalysts.8 Endeavors have been made to convert these C₁ products to C₂ species via concentration of C₁ intermediates on the catalyst

surfaces $^{11-14}$ and delicate modulation of electronic structure of the electrocatalysts. $^{15-18}$ It is clear through these efforts that the critical challenge in forming C2+ products lies in the control of C-C coupling, which is potential-independent and displays sluggish kinetics at room temperature. This inherent feature can help rationalize the finding that thermocatalytic CO₂RR tends to afford a higher yield of C2+ products than the electrocatalytic processes. 19,20 Therefore, conceptual breakthroughs are warranted to address the kinetic limitations of C-C coupling during electrochemical CO₂RR.

A common strategy to address this difficulty is the chemical modification of catalytic centers by doping or solid-solution alloying, which has been widely adopted in the design of Cubased heterogeneous catalysts for CO₂RR. 15,21-27 Cu is renowned for its promising selectivity toward C₂₊ products. On the Cu surface, C-C coupling was believed to proceed via the dimerization of two *CO intermediates, 28-30 the kinetics of which could benefit from the coexistence of $Cu^{\delta +}$ and Cu^0 sites

Received: November 16, 2022 Revised: January 27, 2023 Published: February 9, 2023





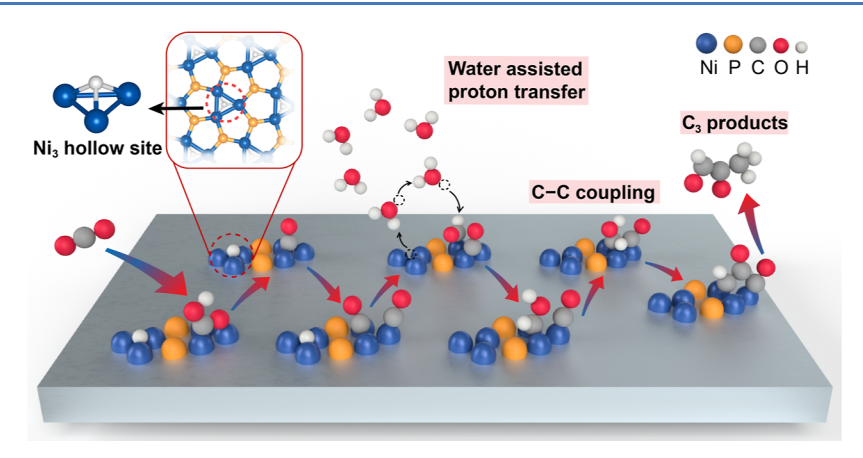


Figure 1. Schematic diagram of the formation path of C_{2+} products on Ni_2P . The surface of Ni_2P is characteristic of densely distributed trinuclear Ni_3 sites, with protons adsorbed at the center of Ni_3 under experimental conditions.

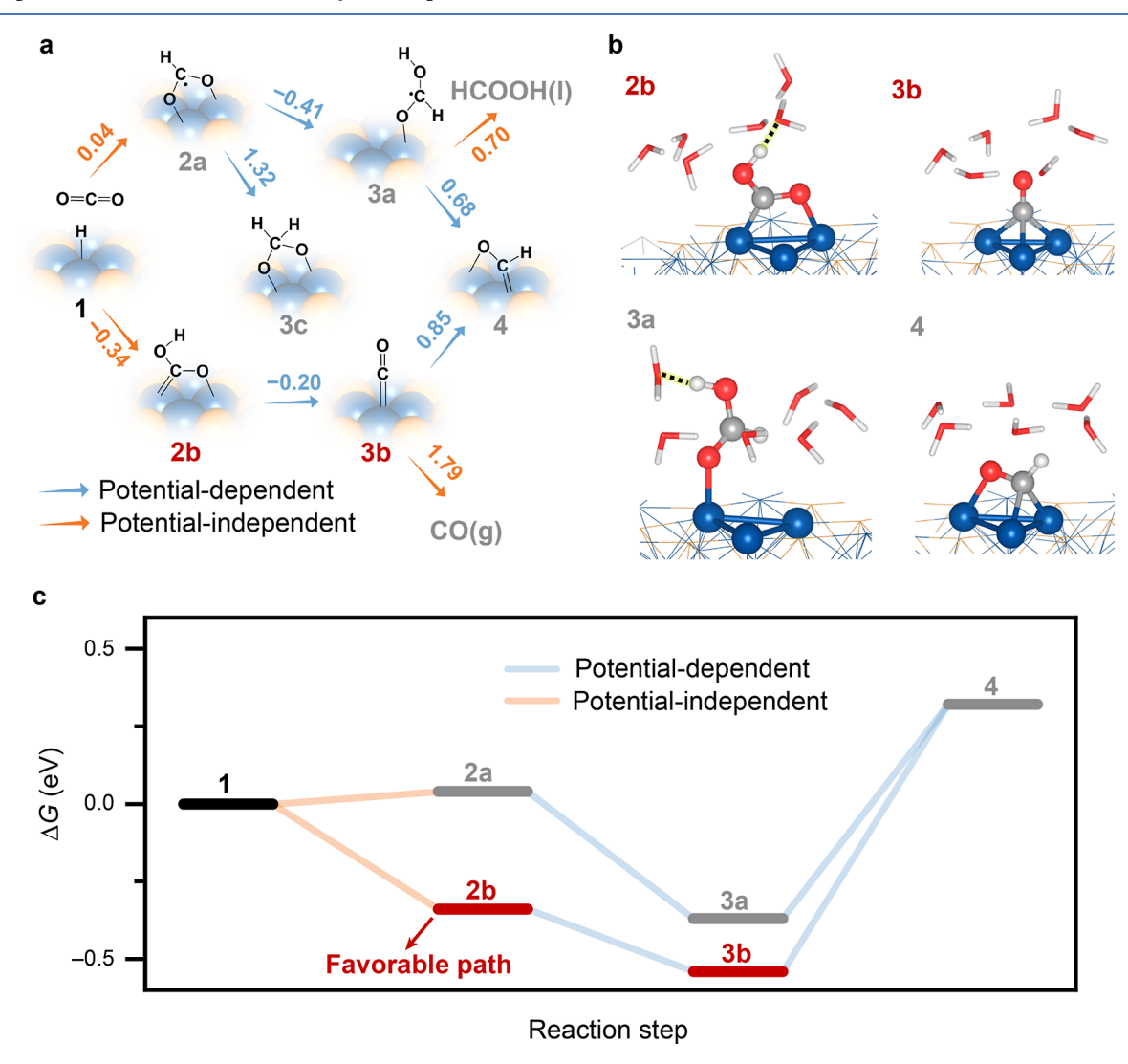


Figure 2. Reaction path of C_1 species. (a) Schematic depiction of reaction pathways for C_1 intermediates. Reaction energy (eV) is shown for each step. The black line between the adsorbate and catalyst surface indicates chemical bonding between the corresponding atoms. (b) Structures of representative C_1 intermediates in the explicit water hexamer model. The black dashed line indicates the hydrogen bond. Color code: nickel, blue; oxygen, red; hydrogen, white; carbon, gray. (c) Free energy diagram for the reaction routes to C_1 intermediates at 0 V vs RHE.

at the catalytic center.^{23,31} Recent studies showed that main-group element dopants could increase the FE for C_2 hydrocarbons to an impressive $\sim 80\%$, ^{15,24} although a sufficiently

negative potential, usually over $-0.7~{\rm V}$ versus reversible hydrogen electrode (RHE) is necessary.

As compared to the compositional approach, strategies based on microstructural control are much rarer. Recently, notable

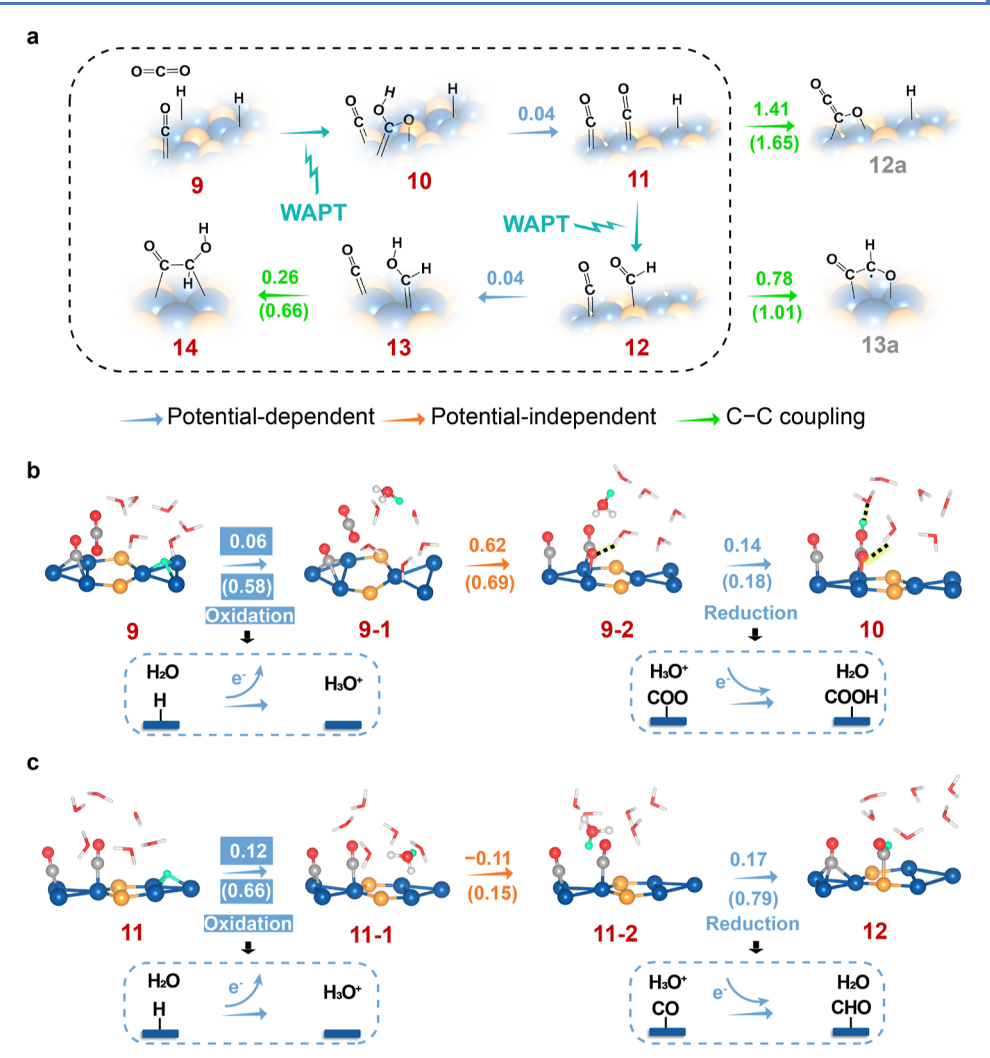


Figure 3. Reaction path of C_2 species. (a) Schematic depiction of reaction pathways for C_2 intermediates. Activation energy barriers (eV) are shown in bracket. Intermediates in the dashed frame are related to the feasible path for the formation of C_{2+} products. WAPT process in forming (b) *CO + *COOH and (c) *CO + *CHO via the proton relay in the water hexamer. The transferred proton is highlighted by the green sphere. The hydrogen bond is highlighted by the dashed black line.

accomplishments were made by using trinuclear Cu₃ clusters stabilized by functional groups as electrocatalysts for CO₂RR,³² which can reach an FE of 91% for CO₂-to-C₂ conversion at −0.7 V versus RHE. Each catalytic center is composed of three embedded Cu atoms, providing adsorption sites for at least two carbon species in close vicinity. In contrast to single atom catalysts 33 that produce mainly C_1 products, $^{34-36}$ such a spatially confined multi-center structure $^{32,37-40}$ is conducive to the coupling reactions because the constrained distance between adsorbates at the catalytic center will offer ample opportunities for their encounter. We speculate that this type of microstructural configuration might be adapted in inorganic crystalline materials in order to facilitate access to C₂₊ products. Intriguingly, a recent report⁴¹ identified Ni₂P as an electrocatalyst with high C2+ selectivity, and this compound is well characteristic of trinuclear Ni₃ sites, resembling the abovementioned trinuclear Cu₃ clusters. The trinuclear Ni₃ structure in Ni₂P is likely essential to the extraordinary performance of >98% FE toward C₃ and C₄ products at 0.01 V versus RHE. Traditionally, only the copper-based catalysts are used for the generation of C2+ products. Ni2P and the recently reported partially oxidized nickel⁴² have demonstrated that Ni-based catalysts are also capable of producing multi-carbon products.

Moreover, these Ni_3 sites of Ni_2P are isolated by P atoms but are not distant from each other, which leads to a multi-center scenario in a higher hierarchy level where the synergy between neighboring trinuclear sites may arise. Nevertheless, it is still unclear from a microscopic point of view as to how these multi-center configurations contribute to the C–C coupling process. With the ongoing research in CO_2RR , a detailed mechanistic understanding in this regard would be vital and increasingly meaningful for the design of C_{2+} -selective electrocatalysts.

In this work, we employ a Ni_2P crystal as a platform to study the role of multi-center catalytic sites on the efficiency of C-C coupling. Leveraging density functional theory calculations, we find that the trinuclear Ni_3 site can reversibly trap protons at the surface and enable co-adsorption of two closely located CO molecules after facile reduction of CO_2 to CO (Figure 1). The hydrogen-bonding network of water molecules above two adjacent trinuclear sites can facilitate the transfer of surface proton from one site to the adsorbates on the other site, leading to further reduction of the *CO intermediates. After this hydrogenation step, two C_1 intermediates on the Ni_3 site can readily combine, with a much lower activation energy than that of $^*CO-^*CO$ dimerization. This promotion is rationalized by the filling of antibonding orbitals of the CO molecule and the

radical nature of the corresponding carbon species, which can be generalized to the analysis on other catalysts. Collectively, we demonstrate that the multi-center microstructure of closely distributed trinuclear sites engenders a high cooperativity for efficient C-C coupling in electrochemical CO_2RR

RESULTS AND DISCUSSION

 Ni_2P Crystal Surface and the Pathways to C_1 Intermediates. We start with the investigation of stable termination for the $Ni_2P(0001)$ crystal surface, which was reported to be one of the dominant low-index surfaces. According to the calculated Pourbaix diagram (Figure S2), a configuration of $Ni_3P_2 + H$ is identified to be the ground-state surface structure for neutral aqueous environment (pH ranging between 7 and 8) at 0 V versus RHE, in a case close to the experimental conditions. This structure features an architecture of densely distributed trinuclear Ni_3 sites, on each of which there stands a proton adsorbate at the hollow position (Figure 1). The hydrogenated surface termination is in agreement with a previous study⁴⁴ emphasizing the aqueous surface stability of Ni_2P crystal during hydrogen evolution reaction (HER).

Based on the Ni_3P_2 + H surface configuration, we examine the reaction path of CO₂RR for the formation of C₁ intermediates, which is a prerequisite for C₂₊ products. CO₂RR begins with the hydrogenation of CO₂ to form either *HCOO (2a) or *COOH (2b) at the catalytic center (Figure 2a, detailed structures shown in Figure S3). These elementary steps are accomplished by direct transfer of the surface proton on the Ni₃ site to the adsorbed CO2. The *HCOO species shows lower formation energy than *COOH if we do not consider the contribution from hydrogen bonds, which is consistent with a recent work.⁴³ However, if we place a water hexamer, which has been previously recognized as one of the possible constitutional units of interfacial water, 46,47 near the reaction intermediates so as to take into account the hydrogen-bonding interaction (Figures 2b,c and S4 and Table S4), the formation of *COOH would be more energetically favorable instead. Given that several recent reports^{30,48-54} have pointed out the strong contribution of hydrogen bonds to the reduction mechanism of CO₂, we choose to employ the water hexamer model in the rest of our work, and as will be shown below, this model is indispensable for the interpretation of the cooperativity between the Ni₃ catalytic centers.

The further hydrogenation of *HCOO generates *HCOOH (3a) with an exothermic reaction energy, while the desorption of *HCOOH to produce a formic acid consumes an energy of 0.70 eV, which can be regarded as the main attribute to the low FE (<5% at all potentials)⁴¹ of formic acid observed in previous experiments. Similar to *HCOO, the formation of *CO (3b) is exothermic while its desorption is highly endothermic. We note that both *HCOOH and *CO could not be hydrogenated into *COH because the *COH configuration is kinetically unstable (Figure S6). The formation of *CHO (4) is also electrochemically unfavorable due to the considerable energy inputs for $3a \rightarrow$ 4 and 3b \rightarrow 4 steps. Therefore, C₁ intermediates with higher hydrogenation degree than HCOOH/CO will hardly be formed in the experimental conditions of 0.01 V versus RHE. In this scenario, *CO can be perceived as a critical C₁ intermediate that has to be bypassed in the formation path of C_{2+} products.

Pathways to C₂ Intermediates. We then proceed to investigate the reduction of the second CO_2 on a Ni_3 site and the subsequent C-C coupling process (Figure 3a, detailed structures shown in Figure S7). Due to the presence of an

already formed *CO at this catalytic center, a relatively strong steric hindrance effect will be exerted on the adsorption of the second CO₂ molecule, thus leading to a high energy input (0.32 eV) for its electrochemical hydrogenation (Figure S8). However, given that the surface protons captured by Ni₃ sites may participate in the reaction, we here propose another possible pathway for the hydrogenation of the second CO₂ molecule (Figure 3b). We note that the water hexamer at the surface could build a proton relay between the surface protons and the reaction intermediates under the Grotthuss proton transfer mechanism. 55,56 This water-assisted proton transfer (WAPT) process involves the detachment and transfer of the surface proton to a nearby water molecule $(9 \rightarrow 9-1)$, the hopping of another proton from this hydronium to one of its neighboring water molecules $(9-1 \rightarrow 9-2)$, and finally the hydrogenation of *CO2 with proton received from the hydrogen-bonding network (9-2 \rightarrow 10). Unlike the first and the last steps, the $9-1 \rightarrow 9-2$ step is potential-independent with a kinetic barrier of 0.69 eV. Importantly, the $9 \rightarrow 9-1$ step corresponds to an electrochemical oxidation reaction (*H + $H_2O \rightarrow * + H_3O^+ + e^-$) that requires a potential of 0.06 V to become exothermic, while the $9-2 \rightarrow 10$ step corresponds to an electrochemical reduction reaction (* $CO_2 + H_3O^+ + e^- \rightarrow$ *COOH + H_2O) with a limiting potential of -0.14 V. The counterbalance between both steps implies that an operating potential close to the experimental value (10 mV vs RHE) is desirable to drive the WAPT process. Therefore, the WAPT process is more energetically favorable than direct electrochemical hydrogenation of the second CO₂ molecule (requiring -0.32 V vs RHE). Moreover, we would like to note that there is an intrinsic link between the kinetics of the WAPT process and the formation of hydronium ion at the interface, which means a nontrivial role for the pH of the solution in regulating the WAPT process on Ni₂P.

In the co-adsorption configuration of two *CO(11), one of the CO molecules is located at the bridge site between two Ni atoms, while the other is on top of the third Ni. Their formation into *OCCO (12a) has to overcome an energy barrier of 1.65 eV. Previous study showed that the activation energy for C-C coupling may change according to the electrode potential.⁵⁷ Thus, we examine the potential-dependent activation energy for the formation of *OCCO with the constant potential method proposed by Chan et al. 58,59 We find that even at a very negative potential (-1 V vs RHE), the formation of *OCCO is extremely difficult with an activation energy of 1.49 eV (Figure S12). Although many studies have invoked *CO dimerization as the C-C coupling step on electrocatalysts, 3,29,60,61 the result presented here suggests that this is a kinetically frustrated process on Ni₃, which has prompted us to propose another reaction path for C-C coupling. As shown in Figure 3c, the WAPT process can also mediate the C-C coupling reaction by forming *CO + *CHO (12) with a maximum energy input of 0.17 eV. Although this configuration still exhibits a high energy barrier for C-C coupling (1.01 eV, $12 \rightarrow 13a$), its further reduction into *CO + *CHOH (13) is remarkably facile, and more importantly, the C-C coupling barrier at this stage is reduced to 0.66 eV (13 \rightarrow 14). Thus, the WAPT mechanism outlines a kinetically controlled and desired pathway to enable hydrogenation of the 2*CO configuration and highlights the cooperative nature of neighboring Ni3 sites in steering the reaction toward C₂₊ products.

Pathways to C₃ and C₄ Products. With the knowledge on the reaction pathways to C_2 species, we can analyze the

ACS Catalysis pubs.acs.org/acscatalysis Research Article

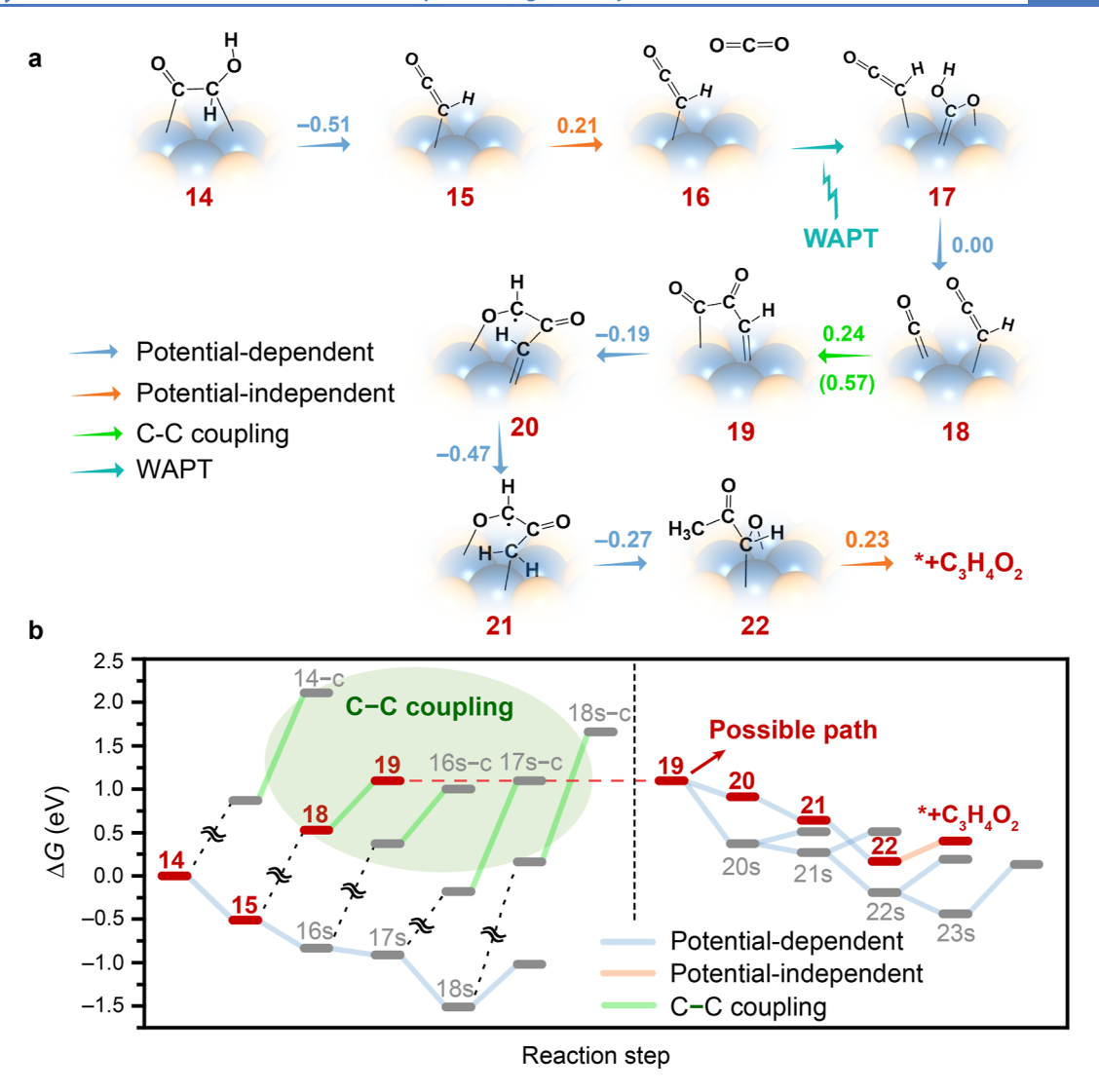


Figure 4. Formation of C_3 product. (a) Schematic depiction of the reaction pathway for a C_3 product. Activation energy barriers (eV) for C–C coupling are shown in bracket. (b) Free energy diagram for the reaction route to a C_3 product at 0 V vs RHE.

mechanism for C₃ formation on Ni₂P. The *CO-CHOH intermediate is chosen as the beginning configuration, and methylglyoxal $(C_3H_4O_2)$, one of the main products observed in the experiments, 41 is taken as the end-point of the C_3 -formation reaction. The most plausible path towards this product and the corresponding free energy profile are displayed in Figure 4 (detailed structures shown in Figure S17). The hydrogenation of *CO-CHOH to other C2 species will proceed through *CH-CO (15), *CH-COH (16), *CH-CHOH (17s), and *CH₂-CHOH (18s) on a downhill energy landscape. Further hydrogenation of 18s is energetically unfavorable (Figure S18) and therefore its reduction products are not taken into consideration in the following analysis. The reduction of the third CO₂ molecule which proceeds via WAPT is similar to the second one (Figure S19), resulting in the formation of an additional *CO at the catalytic site. We then examine the activation barrier for C-C coupling between each of the C2 intermediates (from 14 to 18s, Figure S20) and this *CO adsorbate. The coupling between 15 and *CO turns out to be the most kinetically accessible, with an activation barrier of 0.57 eV to reach *CO-CO-CH (19). Further hydrogenation steps from this C-C coupling product to methylglyoxal via *COH-CO-CH(20), * $COH-CO-CH_2(21)$ and * $COH-CO-CH_3$

(22) are all exothermic, and the desorption of 22 only takes 0.23

We would like to note that 19 can be hydrogenated into various intermediates including *CO-COH-CH (20s), *CHO-COH-CH (21s), *CHO-COH-CH₂ (22s), and *CHO-COH-CH₃ (23s) with a descending energy profile (Figures 4b and S21). Similar to the C_2 species, these C_3 intermediates will likely undergo C-C coupling with the fourth *CO and give rise to C₄ species. A possible reaction pathway is presented in Figure 5 (detailed structures shown in Figure S22). The coupling between 21s and *CO (derived from the fourth CO_2) is kinetically feasible, with an activation barrier of 0.10 eV to reach *CHO-COH-CH-CO (25). This intermediate is then converted into the 2,3-furandial product through a proton tautomerism (26), a hydrogenation step (27), and a cyclization reaction (28). Notably, the intermediate 20s is more stable than **20** (Figure 4b), which creates more opportunities to generate C_4 products than C₃ products. This may be responsible for the higher FE of C₄ products (>70%) in experiments.⁴¹

Overall, while the WAPT process presumably occurs at a potential between 0.12 and -0.17 V versus RHE (according to the $11 \rightarrow 12$ step), all other electrochemical steps for proton coupled electron transfer in forming C_{2+} species require

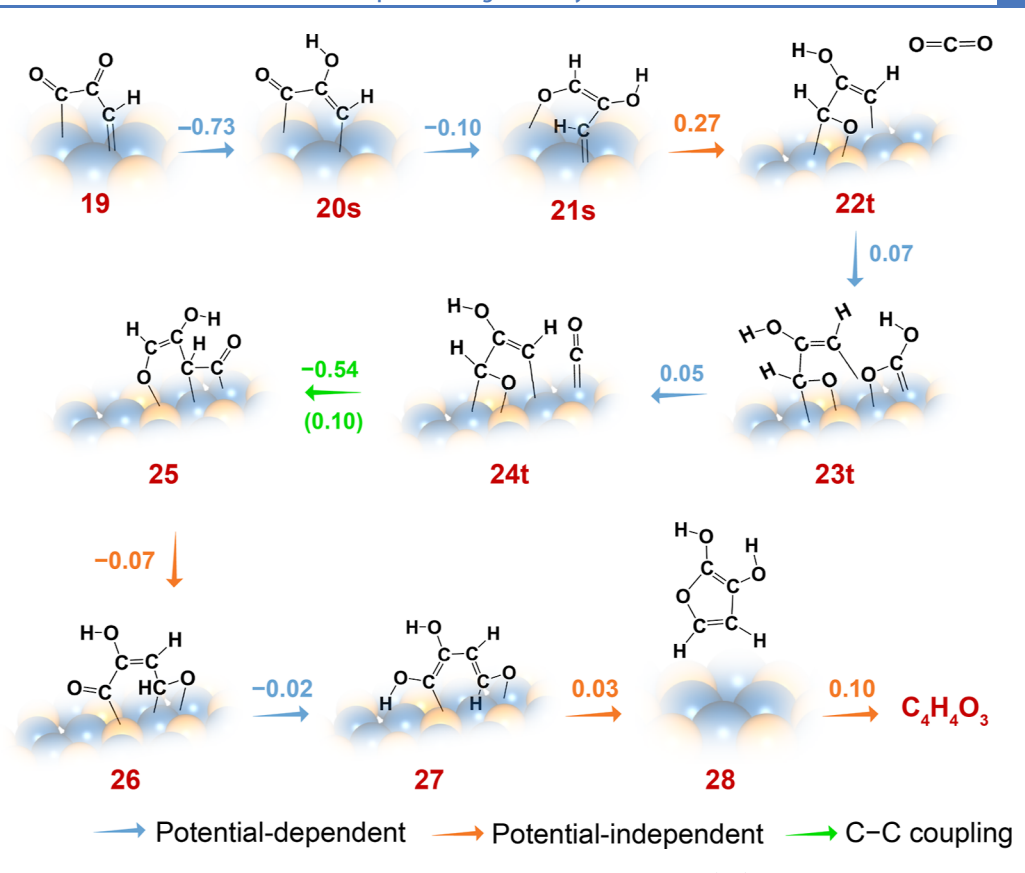


Figure 5. Schematic depiction of reaction pathway for a C₄ product. Activation energy barriers (eV) for C-C coupling are shown in bracket.

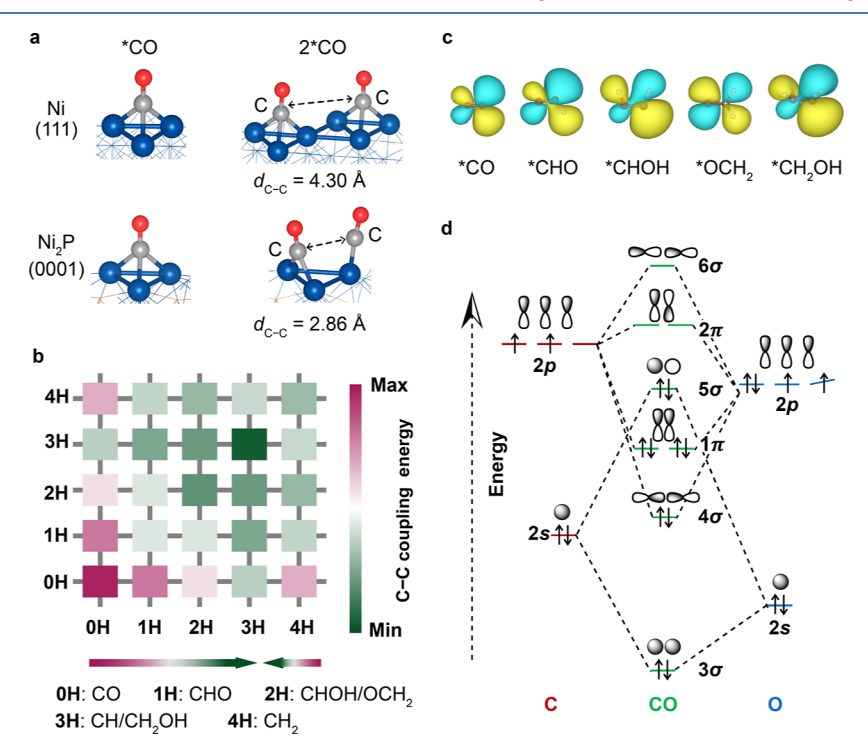


Figure 6. Enabler for facile C-C coupling. (a) Adsorption of *CO and 2*CO on Ni (111) and Ni₂P(0001) surfaces. Shorter distance between *CO adsorbates is obtained at a Ni₃ site as compared to that on a Ni plane. (b) Reaction energy of C-C coupling between different C_1 species. The denotation of (0–4)H corresponds to the hydrogenation degree of *CO. (c) 2π frontier orbitals of *CO, *CHO, *CHOH, *OCH₂, and *CH₂OH. (d) Molecular orbital diagram of a CO molecule.

remarkably low energy input (below 0.1 eV). Despite its inferior kinetics to HER, the $\rm CO_2$ -to- $\rm C_{2+}$ reaction on $\rm Ni_2P$ corresponds to a limiting potential of close to 0 V versus RHE, much more

advantageous than -0.55 V for HER (Figure S24). Hence, at the experimental conditions, CO_2RR will precede over HER, which is in agreement with the experimental results. In the reaction to

multi-carbon products, all the adjacent Ni_3 sites will act as a proton reservoir to boost the hydrogenation of intermediates on the targeted Ni_3 site, leading to acceleration of the C–C coupling steps. This scenario underlines the importance of multi-center cooperativity in circumventing the thermodynamic penalty during the formation of multi-carbon products in CO_2RR .

Cooperative Effect of Ni₃ Centers. In line with the experimental results, 41 the calculations in this work unequivocally confirm that the trinuclear Ni₃ catalytic center endows Ni₂P with a high C₂₊ selectivity in CO₂RR. The multi-center feature of Ni₃ affects C-C coupling in two ways: first, it provides adsorption sites for two C_1 species in a confined space, where the two C atoms binding to the catalyst are to be separated by a substantially shortened distance as compared to that on a metal surface. As shown in Figure 6a, the *CO intermediates on the Ni(111) surface are at least 4.30 Å apart from each other in the stable configuration, while this value is reduced to 2.86 Å on Ni₃. Such a confinement picture is key to catalyze C–C coupling in a more kinetically efficient manner, similar to other structural motifs such as atomic clusters. 32,38,39 While the strong binding of *CO may exert a poison effect for C₁ formation, the different adsorption configurations between both *CO molecules on a Ni₃ site could produce an asymmetric electronic structure for their C atoms (Figure S25), which may facilitate their further hydrogenation and benefit the C–C coupling process afterward. Second, unlike single atom catalysts where the metal centers form strong bonding with the substrate and are oxidized to relatively high valence state, 62-65 the Ni₃ sites in Ni₂P exhibit a delocalized electronic structure that is beneficial for exchanging electrons with the adsorbates, thus mediating their activation and yielding a flattened energy landscape in the CO₂RR process. More importantly, the availability of these labile electrons creates the basis for the accommodation of C₃ and C₄ species, because the electrons can participate in the termination of dangling bonds on the reaction intermediates. We note that most of the C₃ and C₄ intermediates require multiple metalcarbon bonds to stabilize their configuration (Figures S17 and S22). Therefore, it does not come as a surprise that the multicenter microstructure is conducive to the formation of these C_{2+} species, while C-C coupling is barely accessible on single atomic sites.

Apart from the cooperativity among Ni atoms in a single Ni₃ site that ensures the effective accommodation of intermediates, the cooperativity between neighboring Ni₃ sites also proved essential for circumventing the kinetic hindrance in C-C coupling. This cooperativity lies in the WAPT process that permits further hydrogenation of *CO in the co-adsorption configuration. To understand why C-C coupling is promoted upon further hydrogenation of the C_1 intermediates, we examine all the C-C coupling processes that involve *CO, *CHO, *CHOH, *OCH2, *CH2OH, *CH, and *CH2. For clarity of discussions, here we call *CO intermediate "0H" and its subsequently hydrogenated species *CHO "1H". Likewise, the rest of the intermediates can be designated as "2H", "3H", or "4H" according to the hydrogenation degree. The reaction energy for each pair of these C₁ species is displayed in Figure 6b (details given in Table S5 and Figure S26). For species with the same hydrogenation degree, we selected the one with the lowest reaction energy. Apparently, a descending trend of reaction energy is shown from "0H" to "3H": the higher degree of hydrogenation both C_1 species undergo, the smaller the energy consumption will be in C-C coupling. This trend is correlated

with the filling of antibonding orbitals of the CO molecule. In Figure 6c, we show that the 2π molecule orbitals of *CHO, *CHOH, *OCH₂, and *CH₂OH closely resemble that of *CO, which corresponds to the lowest unoccupied molecular orbital (LUMO) of the CO molecule with an antibonding character (Figure 6d). The addition of electrons to the 2π orbital will impair the C–O bonding, giving rise to a radical nature that promotes the C–C coupling efficiency. This radical nature is also witnessed in *CH and *CH₂, with the former being more reactive, as inferred from the Bader charge analysis (Table S6) that reveal a more open-shell electronic configuration for the C atom in *CH than in *CH₂. Therefore, the evolution of C–C coupling kinetics as a function of the hydrogenation degree can be seen as a result of the variation in radical nature of both coadsorbed C₁ species.

As a final remark, we note that Fe₂P, which is isostructural with Ni₂P, was recently reported as a selective electrocatalyst for CO_2 conversion into C_3 and C_4 products. ⁶⁶ It can be deduced that the densely distributed trinuclear motif is an ideal structural basis to steer the reactions along the C–C coupling pathway. The cooperativity between neighboring trinuclear catalytic centers is rooted in the WAPT process, which is the ratelimiting step of the CO_2 reduction on Ni₂P. We therefore envisage that by capitalizing on proper molecular proton mediators ^{67–69} to modulate proton transfer at the interfaces, this multi-center catalytic scheme may advance to an optimal level of efficiency for C_{2+} -selective electroreduction of CO_2 .

CONCLUSIONS

In summary, we have discovered that the superior selectivity of the Ni₂P electrocatalyst toward C₂₊ products in CO₂RR is attributable to the multi-center cooperativity of the densely distributed trinuclear Ni₃ sites at the surface. This cooperativity manifests itself in two hierarchical levels. First, the multiple adsorption sites at each isolated Ni₃ catalytic center can offer a suitable accommodation for both C1 and C2+ species, contributing to increased opportunities for C-C coupling and reduction of the required energy input. Second, the transfer of surface protons between neighboring Ni₃ sites via the WAPT mechanism can assist in the further hydrogenation of *CO intermediates in the co-adsorption configurations, thus lowering the activation barrier for C–C coupling to a substantial degree. Our results reveal a clear strategy for the microstructural design of CO₂RR electrocatalysts, where the multi-center cooperativity could serve as an adaptive regulatory control for the selective access of C₂₊ products.

ASSOCIATED CONTENT

Supporting Information

The Supporting Information is available free of charge at https://pubs.acs.org/doi/10.1021/acscatal.2c05611.

Details in simulation model, equations for the calculations of surface reconstruction, experimental standard formation free energy of solid and aqueous Ni and P species, Pourbaix diagram, free energy of surface species, standard electrochemical potentials, optimized structures, Gibbs free energy change, possible reduction reaction pathways, structural optimization process, potential-dependent activation barriers, energy barriers in WAPT process, and Bader charges (PDF)

AUTHOR INFORMATION

Corresponding Authors

Shunning Li — School of Advanced Materials, Peking University, Shenzhen Graduate School, Shenzhen 518055, China; Chemistry and Chemical Engineering Guangdong Laboratory, Shantou 515031, China; Orcid.org/0000-0002-5381-6025; Email: lisn@pku.edu.cn

Feng Pan — School of Advanced Materials, Peking University, Shenzhen Graduate School, Shenzhen 518055, China; orcid.org/0000-0002-8216-1339; Email: panfeng@pku.edu.cn

Authors

Shisheng Zheng — School of Advanced Materials, Peking University, Shenzhen Graduate School, Shenzhen 518055, China

Xianhui Liang — School of Advanced Materials, Peking University, Shenzhen Graduate School, Shenzhen 518055, China

Junjie Pan – School of Advanced Materials, Peking University, Shenzhen Graduate School, Shenzhen 518055, China

Kang Hu - School of Advanced Materials, Peking University, Shenzhen Graduate School, Shenzhen 518055, China

Complete contact information is available at: https://pubs.acs.org/10.1021/acscatal.2c05611

Author Contributions

§S.Z. and X.L. contributed equally to this work.

Notes

The authors declare no competing financial interest.

ACKNOWLEDGMENTS

The authors acknowledge financial support from the Guangdong Basic and Applied Basic Research Foundation (2020A1515110843), Young S&T Talent Training Program of Guangdong Provincial Association for S&T (SKXRC202211), Chemistry and Chemical Engineering Guangdong Laboratory (grant no. 1922018), Soft Science Research Project of Guangdong Province (no. 2017B030301013), National Natural Science Foundation of China (22109003), Natural Science Foundation of Shenzhen (JCYJ20190813110605381), and the Major Science and Technology Infrastructure Project of Material Genome Bigscience Facilities Platform supported by Municipal Development and Reform Commission of Shenzhen.

■ REFERENCES

- (1) Østergaard, P. A.; Duic, N.; Noorollahi, Y.; Mikulcic, H.; Kalogirou, S. Sustainable development using renewable energy technology. *Renewable Energy* **2020**, *146*, 2430–2437.
- (2) Pregger, T.; Schiller, G.; Cebulla, F.; Dietrich, R.-U.; Maier, S.; Thess, A.; Lischke, A.; Monnerie, N.; Sattler, C.; Clercq, P. L.; Rauch, B.; Köhler, M.; Severin, M.; Kutne, P.; Voigt, C.; Schlager, H.; Ehrenberger, S.; Feinauer, M.; Werling, L.; Zhukov, V. P.; Kirchberger, C.; Ciezki, H. K.; Linke, F.; Methling, T.; Riedel, U.; Aigner, M. Future Fuels—Analyses of the Future Prospects of Renewable Synthetic Fuels. *Energies* **2019**, *13*, 138.
- (3) Garza, A. J.; Bell, A. T.; Head-Gordon, M. Mechanism of CO₂ Reduction at Copper Surfaces: Pathways to C₂ Products. *ACS Catal.* **2018**, *8*, 1490–1499.
- (4) Yang, K. D.; Lee, C. W.; Jin, K.; Im, S. W.; Nam, K. T. Current Status and Bioinspired Perspective of Electrochemical Conversion of ${\rm CO_2}$ to a Long-Chain Hydrocarbon. *J. Phys. Chem. Lett.* **2017**, *8*, 538–545.

- (5) Schouten, K. J.; Calle-Vallejo, F.; Koper, M. T. A step closer to the electrochemical production of liquid fuels. *Angew. Chem., Int. Ed.* **2014**, 53, 10858–10860.
- (6) Zhang, W.; Hu, Y.; Ma, L.; Zhu, G.; Wang, Y.; Xue, X.; Chen, R.; Yang, S.; Jin, Z. Progress and Perspective of Electrocatalytic CO₂ Reduction for Renewable Carbonaceous Fuels and Chemicals. *Adv. Sci.* **2018**, *5*, 1700275.
- (7) Zhu, P.; Wang, H. High-purity and high-concentration liquid fuels through CO₂ electroreduction. *Nat. Catal.* **2021**, *4*, 943–951.
- (8) Zhou, X.; Shan, J.; Chen, L.; Xia, B. Y.; Ling, T.; Duan, J.; Jiao, Y.; Zheng, Y.; Qiao, S. Z. Stabilizing Cu(2+) Ions by Solid Solutions to Promote CO2 Electroreduction to Methane. *J. Am. Chem. Soc.* **2022**, 144, 2079–2084.
- (9) Wang, L.; Chen, W.; Zhang, D.; Du, Y.; Amal, R.; Qiao, S.; Wu, J.; Yin, Z. Surface strategies for catalytic CO_2 reduction: from two-dimensional materials to nanoclusters to single atoms. *Chem. Soc. Rev.* **2019**, *48*, 5310–5349.
- (10) Zhu, Y.; Yang, X.; Peng, C.; Priest, C.; Mei, Y.; Wu, G. Carbon-Supported Single-Atom Catalysts: Carbon-Supported Single Metal Site Catalysts for Electrochemical CO₂ Reduction to CO and Beyond (Small 16/2021). Small 2021, 17, 2170073.
- (11) Zhang, T.; Bui, J. C.; Li, Z.; Bell, A. T.; Weber, A. Z.; Wu, J. Highly selective and productive reduction of carbon dioxide to multicarbon products via in situ CO management using segmented tandem electrodes. *Nat. Catal.* **2022**, *5*, 202–211.
- (12) Zhuang, T. T.; Pang, Y.; Liang, Z.-Q.; Wang, Z.; Li, Y.; Tan, C.-S.; Li, J.; Dinh, C. T.; De Luna, P.; Hsieh, P.-L.; Burdyny, T.; Li, H.-H.; Liu, M.; Wang, Y.; Li, F.; Proppe, A.; Johnston, A.; Nam, D.-H.; Wu, Z.-Y.; Zheng, Y.-R.; Ip, A. H.; Tan, H.; Chen, L.-J.; Yu, S.-H.; Kelley, S. O.; Sinton, D.; Sargent, E. H. Copper nanocavities confine intermediates for efficient electrosynthesis of \mathbf{C}_3 alcohol fuels from carbon monoxide. *Nat. Catal.* **2018**, *1*, 946–951.
- (13) Li, F.; Li, Y. C.; Wang, Z.; Li, J.; Nam, D.-H.; Lum, Y.; Luo, M.; Wang, X.; Ozden, A.; Hung, S.-F.; Chen, B.; Wang, Y.; Wicks, J.; Xu, Y.; Li, Y.; Gabardo, C. M.; Dinh, C.-T.; Wang, Y.; Zhuang, T.-T.; Sinton, D.; Sargent, E. H. Cooperative CO₂-to-ethanol conversion via enriched intermediates at molecule—metal catalyst interfaces. *Nat. Catal.* **2019**, *3*, 75–82.
- (14) Louisia, S.; Kim, D.; Li, Y.; Gao, M.; Yu, S.; Roh, I.; Yang, P. The presence and role of the intermediary CO reservoir in heterogeneous electroreduction of CO₂. *Proc. Natl. Acad. Sci. U.S.A.* **2022**, *119*, No. e2201922119.
- (15) Zhou, Y.; Che, F.; Liu, M.; Zou, C.; Liang, Z.; De Luna, P.; Yuan, H.; Li, J.; Wang, Z.; Xie, H.; Li, H.; Chen, P.; Bladt, E.; Quintero-Bermudez, R.; Sham, T. K.; Bals, S.; Hofkens, J.; Sinton, D.; Chen, G.; Sargent, E. H. Dopant-induced electron localization drives CO₂ reduction to C₂ hydrocarbons. *Nat. Chem.* **2018**, *10*, 974–980.
- (16) Zhong, M.; Tran, K.; Min, Y.; Wang, C.; Wang, Z.; Dinh, C. T.; De Luna, P.; Yu, Z.; Rasouli, A. S.; Brodersen, P.; Sun, S.; Voznyy, O.; Tan, C. S.; Askerka, M.; Che, F.; Liu, M.; Seifitokaldani, A.; Pang, Y.; Lo, S. C.; Ip, A.; Ulissi, Z.; Sargent, E. H. Accelerated discovery of CO₂ electrocatalysts using active machine learning. *Nature* **2020**, *581*, 178–183.
- (17) Zhuang, T. T.; Liang, Z. Q.; Seifitokaldani, A.; Li, Y.; De Luna, P.; Burdyny, T.; Che, F.; Meng, F.; Min, Y.; Quintero-Bermudez, R.; Dinh, C. T.; Pang, Y.; Zhong, M.; Zhang, B.; Li, J.; Chen, P.-N.; Zheng, X.-L.; Liang, H.; Ge, W.-N.; Ye, B.-J.; Sinton, D.; Yu, S.-H.; Sargent, E. H. Steering post-C—C coupling selectivity enables high efficiency electroreduction of carbon dioxide to multi-carbon alcohols. *Nat. Catal.* **2018**, *1*, 421–428.
- (18) Wang, X.; Wang, Z.; Zhuang, T. T.; Dinh, C. T.; Li, J.; Nam, D. H.; Li, F.; Huang, C. W.; Tan, C. S.; Chen, Z.; Chi, M.; Gabardo, C. M.; Seifitokaldani, A.; Todorović, P.; Proppe, A.; Pang, Y.; Kirmani, A. R.; Wang, Y.; Ip, A. H.; Richter, L. J.; Scheffel, B.; Xu, A.; Lo, S. C.; Kelley, S. O.; Sinton, D.; Sargent, E. H. Efficient upgrading of CO to C₃ fuel using asymmetric C-C coupling active sites. *Nat. Commun.* **2019**, *10*, 5186.

- (19) Jiang, Y.; Long, R.; Xiong, Y. Regulating C-C coupling in thermocatalytic and electrocatalytic CO_x conversion based on surface science. *Chem. Sci.* **2019**, *10*, 7310–7326.
- (20) Das, S.; Pérez-Ramírez, J.; Gong, J.; Dewangan, N.; Hidajat, K.; Gates, B. C.; Kawi, S. Core-shell structured catalysts for thermocatalytic, photocatalytic, and electrocatalytic conversion of CO₂. *Chem. Soc. Rev.* **2020**, *49*, 2937–3004.
- (21) Raciti, D.; Wang, C. Recent Advances in CO₂ Reduction Electrocatalysis on Copper. ACS Energy Lett. **2018**, *3*, 1545–1556.
- (22) Nitopi, S.; Bertheussen, E.; Scott, S. B.; Liu, X.; Engstfeld, A. K.; Horch, S.; Seger, B.; Stephens, I. E. L.; Chan, K.; Hahn, C.; Nørskov, J. K.; Jaramillo, T. F.; Chorkendorff, I. Progress and Perspectives of Electrochemical CO₂ Reduction on Copper in Aqueous Electrolyte. *Chem. Rev.* **2019**, *119*, 7610–7672.
- (23) Ye, W.; Guo, X.; Ma, T. A review on electrochemical synthesized copper-based catalysts for electrochemical reduction of CO₂ to C₂₊ products. *Chem. Eng. J.* **2021**, 414, 128825.
- (24) Ma, W.; Xie, S.; Liu, T.; Fan, Q.; Ye, J.; Sun, F.; Jiang, Z.; Zhang, Q.; Cheng, J.; Wang, Y. Electrocatalytic reduction of CO₂ to ethylene and ethanol through hydrogen-assisted C–C coupling over fluorine-modified copper. *Nat. Catal.* **2020**, *3*, 478–487.
- (25) Vasileff, A.; Xu, C.; Jiao, Y.; Zheng, Y.; Qiao, S. Z. Surface and Interface Engineering in Copper-Based Bimetallic Materials for Selective CO₂ Electroreduction. *Chem* **2018**, *4*, 1809–1831.
- (26) Vasileff, A.; Zhu, Y.; Zhi, X.; Zhao, Y.; Ge, L.; Chen, H. M.; Zheng, Y.; Qiao, S. Z. Electrochemical Reduction of CO₂ to Ethane through Stabilization of an Ethoxy Intermediate. *Angew. Chem., Int. Ed. Engl.* **2020**, *59*, 19649–19653.
- (27) Zhi, X.; Vasileff, A.; Zheng, Y.; Jiao, Y.; Qiao, S.-Z. Role of oxygen-bound reaction intermediates in selective electrochemical CO₂ reduction. *Energy Environ. Sci.* **2021**, *14*, 3912–3930.
- (28) Montoya, J. H.; Shi, C.; Chan, K.; Nørskov, J. K. Theoretical Insights into a CO Dimerization Mechanism in CO₂ Electroreduction. *J. Phys. Chem. Lett.* **2015**, *6*, 2032–2037.
- (29) Goodpaster, J. D.; Bell, A. T.; Head-Gordon, M. Identification of Possible Pathways for C-C Bond Formation during Electrochemical Reduction of CO₂: New Theoretical Insights from an Improved Electrochemical Model. *J. Phys. Chem. Lett.* **2016**, *7*, 1471–1477.
- (30) Cheng, T.; Xiao, H.; Goddard, W. A., 3rd. Full atomistic reaction mechanism with kinetics for CO reduction on Cu(100) from ab initio molecular dynamics free-energy calculations at 298 K. *Proc. Natl. Acad. Sci. U.S.A.* 2017, 114, 1795–1800.
- (31) Xiao, H.; Goddard, W. A., 3rd.; Cheng, T.; Liu, Y. Cu metal embedded in oxidized matrix catalyst to promote $\rm CO_2$ activation and CO dimerization for electrochemical reduction of $\rm CO_2$. *Proc. Natl. Acad. Sci. U.S.A.* **2017**, *114*, 6685–6688.
- (32) Xu, H.; Rebollar, D.; He, H.; Chong, L.; Liu, Y.; Liu, C.; Sun, C.-J.; Li, T.; Muntean, J. V.; Winans, R. E.; Liu, D.-J.; Xu, T. Highly selective electrocatalytic CO_2 reduction to ethanol by metallic clusters dynamically formed from atomically dispersed copper. *Nat. Energy* **2020**, *5*, 623–632.
- (33) Qiao, B.; Wang, A.; Yang, X.; Allard, L. F.; Jiang, Z.; Cui, Y.; Liu, J.; Li, J.; Zhang, T. Single-atom catalysis of CO oxidation using Pt₁/FeOx. *Nat. Chem.* **2011**, *3*, 634–641.
- (34) Lü, F.; Bao, H.; Mi, Y.; Liu, Y.; Sun, J.; Peng, X.; Qiu, Y.; Zhuo, L.; Liu, X.; Luo, J. Electrochemical CO_2 reduction: from nanoclusters to single atom catalysts. Sustainable Energy Fuels 2020, 4, 1012–1028.
- (35) Cheng, Y.; Yang, S.; Jiang, S. P.; Wang, S. Supported Single Atoms as New Class of Catalysts for Electrochemical Reduction of Carbon Dioxide. *Small Methods* **2019**, *3*, 1800440.
- (36) Xu, C.; Vasileff, A.; Zheng, Y.; Qiao, S. Z. Recent Progress of 3d Transition Metal Single-Atom Catalysts for Electrochemical CO₂ Reduction. *Adv. Mater. Interfaces* **2020**, *8*, 2001904.
- (37) Jiao, J.; Lin, R.; Liu, S.; Cheong, W. C.; Zhang, C.; Chen, Z.; Pan, Y.; Tang, J.; Wu, K.; Hung, S. F.; Chen, H. M.; Zheng, L.; Lu, Q.; Yang, X.; Xu, B.; Xiao, H.; Li, J.; Wang, D.; Peng, Q.; Chen, C.; Li, Y. Copper atom-pair catalyst anchored on alloy nanowires for selective and efficient electrochemical reduction of CO₂. *Nat. Chem.* **2019**, *11*, 223–228.

- (38) Lu, Y. F.; Dong, L. Z.; Liu, J.; Yang, R. X.; Liu, J. J.; Zhang, Y.; Zhang, L.; Wang, Y. R.; Li, S. L.; Lan, Y. Q. Predesign of Catalytically Active Sites via Stable Coordination Cluster Model System for Electroreduction of CO₂ to Ethylene. *Angew. Chem., Int. Ed. Engl.* **2021**, *60*, 26210–26217.
- (39) Su, X.; Jiang, Z.; Zhou, J.; Liu, H.; Zhou, D.; Shang, H.; Ni, X.; Peng, Z.; Yang, F.; Chen, W.; Qi, Z.; Wang, D.; Wang, Y. Complementary Operando Spectroscopy identification of in-situ generated metastable charge-asymmetry Cu₂-CuN₃ clusters for CO2 reduction to ethanol. *Nat. Commun.* **2022**, *13*, 1322.
- (40) Pei, W.; Zhou, S.; Zhao, J.; Xu, X.; Du, Y.; Dou, S. X. Immobilized trimeric metal clusters: A family of the smallest catalysts for selective CO_2 reduction toward multi-carbon products. *Nano Energy* **2020**, *76*, 105049.
- (41) Calvinho, K. U. D.; Laursen, A. B.; Yap, K. M. K.; Goetjen, T. A.; Hwang, S.; Murali, N.; Mejia-Sosa, B.; Lubarski, A.; Teeluck, K. M.; Hall, E. S.; Garfunkel, E.; Greenblatt, M.; Dismukes, G. C. Selective CO_2 reduction to C_3 and C_4 oxyhydrocarbons on nickel phosphides at overpotentials as low as 10 mV. *Energy Environ. Sci.* **2018**, *11*, 2550–2559.
- (42) Zhou, Y.; Martín, A. J.; Dattila, F.; Xi, S.; López, N.; Pérez-Ramírez, J.; Yeo, B. S. Long-chain hydrocarbons by CO_2 electroreduction using polarized nickel catalysts. *Nat. Catal.* **2022**, *5*, 545–554.
- (43) Kanama, D.; Oyama, S. T.; Otani, S.; Cox, D. F. Photoemission and LEED characterization of Ni₂P(0001). Surf. Sci. **2004**, 552, 8–16.
- (44) Wexler, R. B.; Martirez, J. M. P.; Rappe, A. M. Active Role of Phosphorus in the Hydrogen Evolving Activity of Nickel Phosphide (0001) Surfaces. *ACS Catal.* **2017**, *7*, 7718–7725.
- (45) Banerjee, S.; Kakekhani, A.; Wexler, R. B.; Rappe, A. M. Mechanistic Insights into CO₂ Electroreduction on Ni₂P: Understanding Its Selectivity toward Multicarbon Products. *ACS Catal.* **2021**, *11*, 11706–11715.
- (46) Carrasco, J.; Hodgson, A.; Michaelides, A. A molecular perspective of water at metal interfaces. *Nat. Mater.* **2012**, *11*, 667–674.
- (47) Björneholm, O.; Hansen, M. H.; Hodgson, A.; Liu, L. M.; Limmer, D. T.; Michaelides, A.; Pedevilla, P.; Rossmeisl, J.; Shen, H.; Tocci, G.; Tyrode, E.; Walz, M. M.; Werner, J.; Bluhm, H. Water at Interfaces. *Chem. Rev.* **2016**, *116*, 7698–7726.
- (48) Seifitokaldani, A.; Gabardo, C. M.; Burdyny, T.; Dinh, C. T.; Edwards, J. P.; Kibria, M. G.; Bushuyev, O. S.; Kelley, S. O.; Sinton, D.; Sargent, E. H. Hydronium-Induced Switching between CO₂ Electroreduction Pathways. *J. Am. Chem. Soc.* **2018**, *140*, 3833–3837.
- (49) Cheng, T.; Xiao, H.; Goddard, W. A., 3rd Reaction Mechanisms for the Electrochemical Reduction of CO₂ to CO and Formate on the Cu(100) Surface at 298 K from Quantum Mechanics Free Energy Calculations with Explicit Water. J. Am. Chem. Soc. 2016, 138, 13802—13805.
- (50) Zhao, X.; Liu, Y. Unveiling the Active Structure of Single Nickel Atom Catalysis: Critical Roles of Charge Capacity and Hydrogen Bonding. *J. Am. Chem. Soc.* **2020**, *142*, 5773–5777.
- (51) Cheng, T.; Xiao, H.; Goddard, W. A., 3rd Free-Energy Barriers and Reaction Mechanisms for the Electrochemical Reduction of CO on the Cu(100) Surface, Including Multiple Layers of Explicit Solvent at pH 0. *J. Phys. Chem. Lett.* **2015**, *6*, 4767–4773.
- (52) Ludwig, T.; Gauthier, J. A.; Dickens, C. F.; Brown, K. S.; Ringe, S.; Chan, K.; Nørskov, J. K. Atomistic Insight into Cation Effects on Binding Energies in Cu-Catalyzed Carbon Dioxide Reduction. *J. Phys. Chem. C* **2020**, 124, 24765–24775.
- (53) Ye, Y.; Yang, H.; Qian, J.; Su, H.; Lee, K. J.; Cheng, T.; Xiao, H.; Yano, J.; Goddard, W. A., 3rd; Crumlin, E. J. Dramatic differences in carbon dioxide adsorption and initial steps of reduction between silver and copper. *Nat. Commun.* **2019**, *10*, 1875.
- (54) Lum, Y.; Cheng, T.; Goddard, W. A., 3rd; Ager, J. W. Electrochemical CO Reduction Builds Solvent Water into Oxygenate Products. J. Am. Chem. Soc. 2018, 140, 9337–9340.
- (55) Wolke, C. T.; Fournier, J. A.; Dzugan, L. C.; Fagiani, M. R.; Odbadrakh, T. T.; Knorke, H.; Jordan, K. D.; McCoy, A. B.; Asmis, K.

- R.; Johnson, M. A. Spectroscopic snapshots of the proton-transfer mechanism in water. *Science* **2016**, *354*, 1131–1135.
- (56) Zhao, Q.; Song, A.; Zhao, W.; Qin, R.; Ding, S.; Chen, X.; Song, Y.; Yang, L.; Lin, H.; Li, S.; Pan, F. Boosting the Energy Density of Aqueous Batteries via Facile Grotthuss Proton Transport. *Angew. Chem., Int. Ed. Engl.* **2021**, *60*, 4169–4174.
- (57) Gauthier, J. A.; Lin, Z.; Head-Gordon, M.; Bell, A. T. Pathways for the Formation of C₂₊ Products under Alkaline Conditions during the Electrochemical Reduction of CO₂. ACS Energy Lett. **2022**, 7, 1679–1686.
- (58) Vijay, S.; Gauthier, J. A.; Heenen, H. H.; Bukas, V. J.; Kristoffersen, H. H.; Chan, K. Dipole-Field Interactions Determine the CO₂ Reduction Activity of 2D Fe–N–C Single-Atom Catalysts. *ACS Catal.* **2020**, *10*, 7826–7835.
- (59) Gauthier, J. A.; Dickens, C. F.; Ringe, S.; Chan, K. Practical Considerations for Continuum Models Applied to Surface Electrochemistry. *Chemphyschem* **2019**, *20*, 3074–3080.
- (60) Calle-Vallejo, F.; Koper, M. T. Theoretical considerations on the electroreduction of CO to C₂ species on Cu(100) electrodes. *Angew. Chem., Int. Ed. Engl.* **2013**, 52, 7282–7285.
- (61) Lee, C. W.; Shin, S.-J.; Jung, H.; Nguyen, D. L. T.; Lee, S. Y.; Lee, W. H.; Won, D. H.; Kim, M. G.; Oh, H.-S.; Jang, T.; Kim, H.; Min, B. K.; Hwang, Y. J. Metal—Oxide Interfaces for Selective Electrochemical C—C Coupling Reactions. *ACS Energy Lett.* **2019**, *4*, 2241—2248.
- (62) Yang, H. B.; Hung, S.-F.; Liu, S.; Yuan, K.; Miao, S.; Zhang, L.; Huang, X.; Wang, H.-Y.; Cai, W.; Chen, R.; Gao, J.; Yang, X.; Chen, W.; Huang, Y.; Chen, H. M.; Li, C. M.; Zhang, T.; Liu, B. Atomically dispersed Ni(i) as the active site for electrochemical CO₂ reduction. *Nat. Energy* **2018**, *3*, 140–147.
- (63) Zheng, S.; Zuo, C.; Liang, X.; Li, S.; Pan, F. Valence state of transition metal center as an activity descriptor for CO₂ reduction on single atom catalysts. *J. Energy Chem.* **2021**, *56*, 444–448.
- (64) Liu, D.; He, Q.; Ding, S.; Song, L. Structural Regulation and Support Coupling Effect of Single-Atom Catalysts for Heterogeneous Catalysis. *Adv. Energy Mater.* **2020**, *10*, 2001482.
- (65) Yang, J.; Li, W.; Wang, D.; Li, Y. Electronic Metal-Support Interaction of Single-Atom Catalysts and Applications in Electrocatalysis. *Adv. Mater.* **2020**, 32, No. e2003300.
- (66) Calvinho, K. U. D.; Alherz, A. W.; Yap, K. M. K.; Laursen, A. B.; Hwang, S.; Bare, Z. J. L.; Clifford, Z.; Musgrave, C. B.; Dismukes, G. C. Surface Hydrides on Fe₂P Electrocatalyst Reduce CO₂ at Low Overpotential: Steering Selectivity to Ethylene Glycol. *J. Am. Chem. Soc.* 2021, 143, 21275–21285.
- (67) Liu, X.; Li, B.; Soto, F. A.; Li, X.; Unocic, R. R.; Balbuena, P. B.; Harutyunyan, A. R.; Hone, J.; Esposito, D. V. Enhancing Hydrogen Evolution Activity of Monolayer Molybdenum Disulfide via a Molecular Proton Mediator. *ACS Catal.* **2021**, *11*, 12159–12169.
- (68) Suryanto, B. H. R.; Matuszek, K.; Choi, J.; Hodgetts, R. Y.; Du, H. L.; Bakker, J. M.; Kang, C. S. M.; Cherepanov, P. V.; Simonov, A. N.; MacFarlane, D. R. Nitrogen reduction to ammonia at high efficiency and rates based on a phosphonium proton shuttle. *Science* **2021**, *372*, 1187–1191.
- (69) Wang, T.; Zhang, Y.; Huang, B.; Cai, B.; Rao, R. R.; Giordano, L.; Sun, S.-G.; Shao-Horn, Y. Enhancing oxygen reduction electrocatalysis by tuning interfacial hydrogen bonds. *Nat. Catal.* **2021**, *4*, 753–762.



CAS BIOFINDER DISCOVERY PLATFORM™

BRIDGE BIOLOGY AND CHEMISTRY FOR FASTER ANSWERS

Analyze target relationships, compound effects, and disease pathways

Explore the platform

